

# Deformation behaviour of body centered cubic iron nanopillars containing coherent twin boundaries

G. Sainath\*, B.K. Choudhary†

*Deformation and Damage Modelling Section  
Mechanical Metallurgy Division  
Indira Gandhi Centre for Atomic Research, Kalpakkam  
Tamilnadu-603102, India*

## Abstract

Molecular dynamics simulations were performed to understand the role of twin boundaries on deformation behaviour of body-centred cubic (BCC) iron (Fe) nanopillars. The twin boundaries varying from one to five providing twin boundary spacing in the range 8.5 - 2.8 nm were introduced perpendicular to the loading direction. The simulation results indicated that the twin boundaries in BCC Fe play a contrasting role during deformation under tensile and compressive loadings. During tensile deformation, a large reduction in yield stress was observed in twinned nanopillars compared to perfect nanopillar. However, the yield stress exhibited only marginal variation with respect to twin boundary spacing. On the contrary, a decrease in yield stress with increase in twin boundary spacing was obtained during compressive deformation. This contrasting behaviour originates from difference in operating mechanisms during yielding and subsequent plastic deformation. It has been observed that the deformation under tensile loading was dominated mainly by twin growth mechanism, due to which the twin boundaries offers a negligible resistance to slip of twinning partials. This is reflected in the negligible variation of yield stress as a function of twin boundary spacing. On the other hand, the deformation was dominated by nucleation and slip of full dislocations under compressive loading. The twin boundaries offer a strong repulsive force on full dislocations resulting in the yield stress dependence on twin boundary spacing. Further, it has been observed that the curved twin boundary can acts as a source for full dislocation. The occurrence of twin-twin interaction during tensile deformation and dislocation-twin interaction during compressive deformation were presented and discussed.

**Keywords:** Molecular Dynamics simulations, BCC Fe, Nanopillars, Twin boundaries, Twinning and slip.

---

\*email : sg@igcar.gov.in

†email : bkc@igcar.gov.in

# 1 Introduction

In recent years, the twinned nanopillars or nanowires have drawn growing attention in view of their superior physical properties and potential applications in modern small-scale electronic devices such as nano/micro electro mechanical systems. The twinned nanopillars contain a series of twin boundaries with specified spacing between the boundaries. Twin boundary possesses high symmetry and lowest interface energy along with well-defined boundary plane. The low energy of twin boundaries results in a number of superior properties over conventional grain boundaries. For example, it has been found that the twin boundaries enhance the strength without loss of ductility [1–3], improve fracture toughness and crack resistance [4–6], and increase corrosion resistance and strain rate sensitivity [7]. Moreover, the twin boundaries possess high thermal and mechanical stability [8,9] and high electrical conductivity [10]. The superior mechanical properties of twinned nanopillars have been attributed to unique deformation mechanisms operating in the presence of twin boundaries [11]. In view of this, the materials containing high density of twin boundaries attract huge interest among materials scientists and engineers.

Several experimental and molecular dynamics (MD) simulation studies have been performed to understand the influence of twin boundaries on the strength and deformation behaviour in FCC nanopillars/nanowires [12–16]. Using MD simulations, Cao et al. [12] have shown that in FCC nanopillars, the twin boundaries serve as the strong obstacles for dislocations motion. As a result, the decrease in twin boundary spacing increases the yield strength in orthogonally twinned Cu nanopillars. Apart from obstacle to dislocation motion, the twin boundaries also serve as dislocation source once they lose their coherency at large plastic deformation [12]. This nature of twin boundaries as a dislocation source and also as a glide plane contributes to the improvement in tensile ductility. Zhang and Huang [13] have shown that the twin boundaries do not always strengthen the nanowires. It has been demonstrated that the presence of twin boundaries in square cross-section nanopillars leads to strengthening effect, while in nanopillars with circular cross-sections, softening is observed [13]. Further, the strengthening in twinned FCC nanopillars also depends on the size and aspect ratio [14]. In addition to orthogonally twinned FCC nanopillars, the increase in yield stress is also observed in slanted and vertically twinned FCC nanopillars [15,16]. Using molecular dynamics simulations and in situ experiments, the deformation mechanisms responsible for superior properties and the associated dislocation-twin boundary interactions have been characterised in FCC nanopillars.

Most of the studies reported in the literature have been performed on twinned FCC nanopillars and little attention has been paid to characterise the mechanical behaviour of twinned BCC nanowires/nanopillars. It is well known that the twin boundaries in FCC system coincide with  $\{111\}$  planes, while in BCC systems they coincide with  $\{112\}$  planes [17]. The FCC(111) plane has a closed packed structure and the twin boundary on this plane results from the stacking disorder such as ABCACBA. On the other hand, the BCC(112) plane is not a closed packed structure and the twin boundary consists of stacking disorder on  $\{112\}$  planes with six layers ABCDEFACBDCBA. Because of the different atomic densities and stacking sequence, the twin boundary in BCC system possesses higher energy than the corresponding twin boundary in FCC system [18]. Moreover, the mirror symmetry across the boundary plane is preserved in FCC systems. Whereas in BCC systems, the twin boundary can have either reflection structure, where mirror symmetry is preserved or it can have displaced structure, where the upper grain is displaced with respect to the lower grain by a vector  $1/12\langle 111 \rangle$  [19]. The displaced boundary

no longer possesses the mirror symmetry. In view of different interface energies and twin boundary structures, the effect of twin boundaries in BCC systems may be different than that in FCC systems. For the first time, an attempt has been made in the present investigation to study the influence of twin boundaries on the deformation behaviour under tensile and compressive loadings in BCC nanopillars using atomistic simulations.

An examination of the deformation behaviour of twinned nanopillars also offers valuable insights into twin-twin and dislocation-twin interactions. In FCC metals, the dislocation-twin boundary and twin-twin interactions are well understood, and can be described by the notation of double Thompson tetrahedron [20,21]. Depending on dislocation character and applied stress, various reactions such as dislocation transmission across the twin boundary, sessile stair-rod formation, dislocation incorporation into twin boundaries leading to twin growth or detwinning and dislocation multiplication have been observed in FCC systems [16,20,21]. The absence of such simplified notation and non-planar core of screw dislocations along with the presence of twinning-antitwinning sense on  $\{112\}$  planes make it difficult to understand the dislocations-twin boundary interactions in BCC metals. There are only a couple of studies pertaining to the dislocation-twin and twin-twin interactions in BCC metals [22–24]. In view of the above observations, the present paper is aimed at understanding the role of twin boundaries and the mechanisms responsible for strengthening or softening behaviour in BCC Fe nanopillars. It is also aimed at characterising the twin-twin and dislocation-twin interactions observed during the deformation. The twin boundaries have been introduced perpendicular to the loading direction and number of twin boundaries varied from one to five with corresponding twin boundary spacing in the range 2.8 - 8.5 nm. The stress-strain behaviour and the variations in yield strength and deformation mechanism with respect to twin boundary spacing and loading mode have been discussed.

## 2 MD Simulation details

Molecular dynamics simulations have been carried out in large-scale atomic/molecular massively parallel simulator package [25] and the visualisation of atomic structure is accomplished using AtomEye [26] package with centrosymmetry parameter [27]. The embedded atom method (EAM) potential for BCC Fe given by Mendelev and co-workers [28] has been chosen to describe the interaction between Fe atoms. This potential is widely used to study the deformation behaviour of BCC Fe [29–33]. In order to create twinned nanopillars, the following procedure was adopted. Initially, the single crystal BCC Fe nanopillars of square cross section width ( $d$ ) = 8.5 nm and consisting of about 110,000 atoms oriented in  $\langle 112 \rangle$  axial direction with  $\{110\}$  and  $\{111\}$  as side surfaces was constructed. The nanopillar length ( $l$ ) was twice the cross section width ( $d$ ). Following this, the twin boundaries were introduced by rotating one part of the crystal with respect to other by  $180^\circ$  around  $\langle 112 \rangle$  axis. Following the rotation, the twin boundary forms at their interface on  $\{112\}$  plane. The formed twin boundary is equivalent to a twist boundary lying on  $\{112\}$  plane with a twist angle of  $180^\circ$ . Similar procedure was followed to create more number of twin boundaries. The model system was equilibrated to a temperature of 10 K in NVT ensemble. In all the nanopillars, no periodic boundary conditions were used in any direction. Following the relaxation, the twin boundary having displaced structure was observed [19,31,33,34]. The nanopillars containing one, two, three and five twin boundaries resulted in the twin boundary spacings of 8.5, 5.7, 4.2 and 2.8 nm, respectively. The

BCC Fe nanopillars with different twin boundary spacings considered in this study along with perfect nanopillar are shown in Figure 1. Since the present study focuses on the effect of twin boundary spacing on deformation behaviour and therefore, the effects associated with nanopillar size, aspect ratio and temperature have not been considered. Upon completion of equilibrium process, the deformation under tensile and compressive loadings was carried out in a displacement controlled mode at a constant strain rate of  $1 \times 10^8 \text{ s}^{-1}$  by imposing displacements to atoms along the nanopillar length that varied linearly from zero at the bottom to a maximum value at the top layer. The average stress is calculated from the Virial expression [35].

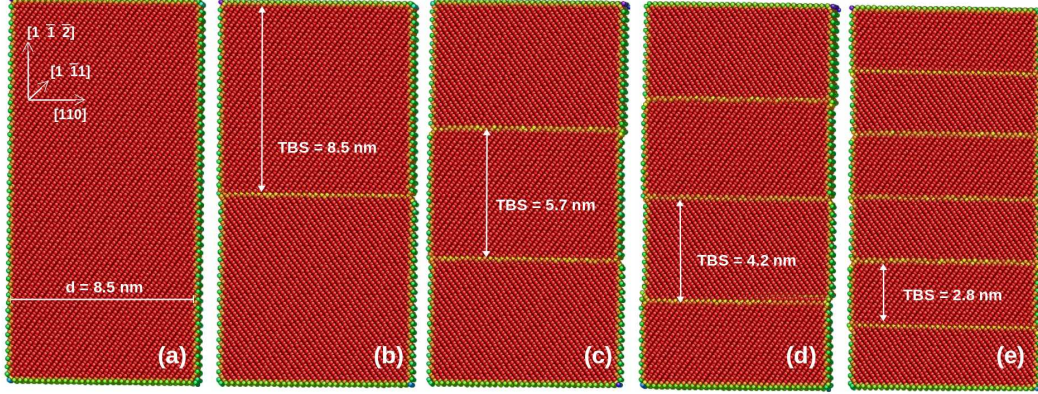


Figure 1: The initial configuration of (a) perfect BCC Fe nanopillar and the nanopillar consisting of (b) one (c) two (d) three and (e) five twin boundaries. The corresponding twin boundary spacings (TBS) of 8.5, 5.7, 4.2 and 2.8 nm are shown. The atoms are coloured according to the centro-symmetry parameter [27].

The Burgers vectors of full dislocations were determined using Dislocation extraction algorithm (DXA) developed by Stukowski [36] as implemented in OVITO [37]. However, the identification of Burgers vector of partial/twinning dislocations gliding on the twin boundary in BCC system is challenging. This is mainly because the Burgers circuit of twinning dislocation passes through the twin boundary at which the crystal orientation changes. Therefore, the reference frame for the Burgers vector analysis is no longer the perfect lattice, but is a bicrystal containing a perfect twin boundary [36]. Due to this difficulty, the DXA or OVITO packages failed to detect the Burgers vectors of partial dislocations and the type of dislocation intersection. We have assigned the Burgers vector of partial/twinning dislocations in BCC Fe based on the experimental observations of Paxton [38]. Generally in BCC systems, the  $1/6\langle 111 \rangle$  type of partial dislocations are responsible for twinning mechanism [17]. Therefore, we have taken  $1/6\langle 111 \rangle$  as the Burgers vector of partial dislocations gliding along the twin boundary. Finally, the type of twin-twin intersection is identified based on the common line of intersection [39]. If  $m$  and  $n$  are the plane normals of the two interacting twins, the intersection type is the vector corresponding to their common intersection line, and is given by the cross product of  $m$  and  $n$  [23].

## 3 Results

### 3.1 Stress-strain behaviour

The stress-strain behaviour of BCC Fe nanopillars under tensile loading containing one, two, three and five twin boundaries along with the perfect nanopillar is shown in Figure 2. All the nanopillars exhibited linear elastic

deformation at small strains followed by nonlinearity at higher strains, i.e.  $\varepsilon > 0.05$ . The modulus evaluated from the linear elastic regime displayed insignificant variations and this indicated that the elastic modulus is not influenced by the presence of twin boundaries. Following elastic deformation, the large and abrupt drop in flow stress signifying the occurrence of yielding in the perfect and twinned nanopillars is seen in Figure 2. In BCC Fe, introduction of twin boundaries resulted in the significant reduction in yield stress compared to that in perfect nanopillar. Similarly, a decrease in the strain to yielding has also been observed in the twinned nanopillars. The yield stress exhibited only marginal variation with respect to twin boundary spacing as shown in Figure 3. For comparison, the yield stress of perfect nanopillar is shown as horizontal line in Figure 3. Following yielding, the perfect nanopillar exhibited nearly a constant and low flow stress during plastic deformation up to large strains. Contrary to this, the nanopillars containing one and two twin boundaries displayed a gradual decrease in the flow stress with increase in plastic deformation. A rapid decrease in flow stress with increase in plastic strain was observed for nanopillars having three and five twin boundaries. Further, the nanopillars having three and five twin boundaries shows higher flow stress with significant fluctuations at low plastic strains. A general decrease in strain to failure has been obtained in the twinned nanopillars compared to that in the perfect nanopillar.

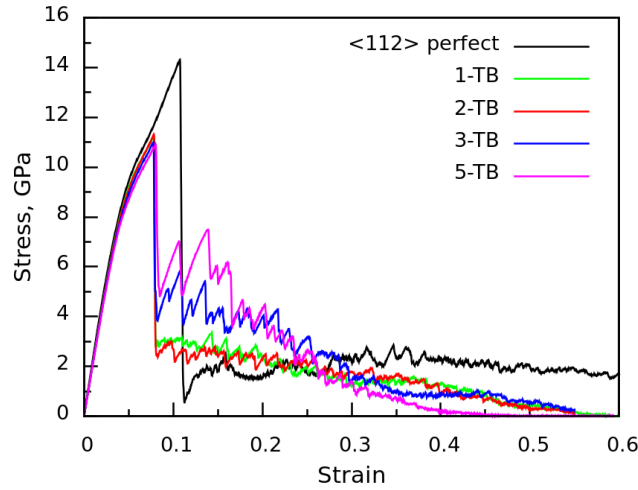


Figure 2: The stress-strain behaviour of BCC Fe nanopillars containing one, two, three and five twin boundaries (TBs) along with stress-strain behaviour of perfect nanopillar under tensile loading.

Figure 4 shows the stress-strain behaviour of perfect and twinned BCC Fe nanopillars under compressive loading. It can be seen that the defect free nanopillar exhibits perfect linear elastic deformation, while the twinned nanopillars display linear elastic deformation at small strains followed by non-linear elastic deformation at high strains. In addition to this, the perfect nanopillar exhibited higher elastic modulus than those observed for twinned nanopillars. Following elastic deformation, the nanopillars displayed yielding characterised by an abrupt drop in flow stress. However, the drop in flow stress during yielding under compressive loading (Figure 4) has been significantly lower than those under tensile loading (Figure 2). Under compressive deformation, decrease in yield stress in the presence of a single twin boundary followed by an increase in yield stress with increase in the number of twin boundaries has been observed. Finally, the yield stress attains a value closer (with three twin boundaries) or marginally higher (with five twin boundaries) than that in the perfect nanopillar (Figure 5). In general, under compressive loading, all the nanopillars displayed large oscillations and gradual decrease in flow

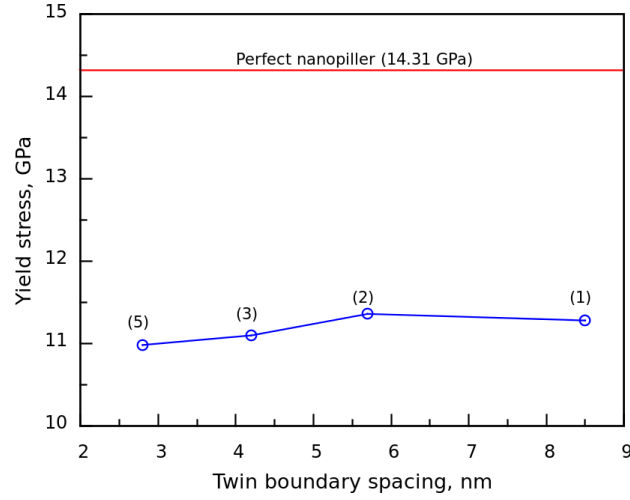


Figure 3: Variation in yield stress as a function of twin boundary spacing in BCC Fe nanopillars under tensile loading. The yield stress of perfect nanopillar is indicated by red line and the number of twin boundaries is shown in small brackets.

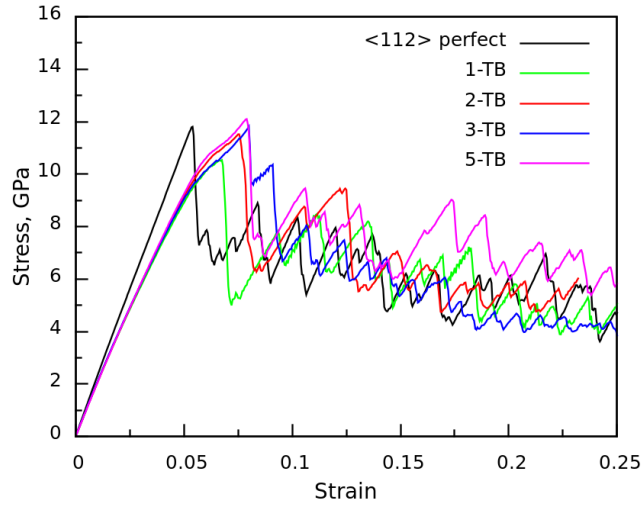


Figure 4: The stress-strain behaviour of BCC Fe nanopillars containing one, two, three and five twin boundaries (TBs) along with stress-strain behaviour of perfect nanopillar under compressive loading.

stress with progressive plastic deformation (Figure 4).

### 3.2 Deformation behaviour under tensile loading

The evolution of atomic configurations at various stages of deformation during the tensile loading of the  $\langle 112 \rangle$  perfect and twinned BCC Fe nanopillars has been analysed using centro-symmetry parameter [27]. It has been observed that the deformation is dominated mainly by the nucleation of twin embryo from the corner during yielding followed by twin growth during plastic deformation. In the detailed investigation performed on  $\langle 112 \rangle$  perfect BCC Fe nanowires, it has been demonstrated that the yielding and subsequent plastic deformation occur by twinning mechanism along with minor dislocation slip activity [33]. Due to deformation twinning, the original  $\langle 112 \rangle$  nanowire with  $\{111\}$  and  $\{110\}$  surfaces transforms to  $\langle 100 \rangle$  nanowire with  $\{100\}$  lateral surfaces [33]. Similar to perfect nanopillar, the deformation in twinned nanopillars is dominated by the twinning and associated partial dislocation mechanism. Figure 6 shows the deformation behaviour under the tensile loading of BCC Fe

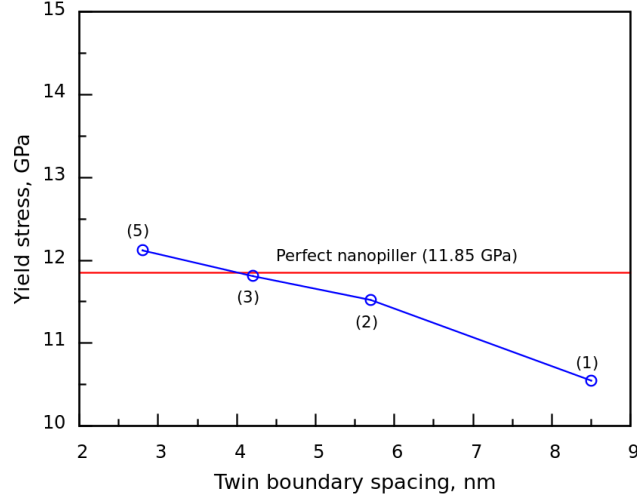


Figure 5: Variation in yield stress as a function of twin boundary spacing in BCC Fe nanopillars under compressive loading. The yield stress of perfect nanopillar is indicated by red line and the number of twin boundaries is shown in small brackets.

nanopillar containing a single twin boundary. The nanopillar yields by the nucleation of a twin embryo from the intersection of surface and the existing twin boundary (Figure 6(a)). Similar yielding behaviour was observed in nanopillars containing higher number of twin boundaries. With small increase in strain, the nucleation and glide of  $1/6 \langle 111 \rangle$  partial dislocation along the initial twin boundary can be seen in Figure 6(b). The glide of partial dislocation leads to the migration of initial twin boundary and thereby changes the twin boundary spacing (Figure 6(c) and (d)). The detailed mechanism of twin boundary formation and the migration of initial twin boundary are shown in Figures 7 and 8 respectively. Initially the  $1/6 \langle 111 \rangle$  partial dislocation nucleates on  $\{112\}$  plane from the corner of the nanowire with a stacking fault behind (Figure 7(a)). Upon increasing deformation, this partial dislocation glides further in  $\langle 111 \rangle$  direction (Figure 7(b)) and an additional  $1/6 \langle 111 \rangle$  partial dislocations nucleates from the intersection of the surface and stacking fault as shown in Figure 7(b) and (c). When twin front reaches the opposite surface, the twin embryo eventually becomes full twin enclosed by two  $\{112\}$  twin boundaries (Figure 7(d)). Following this, the twin grows along the nanowire axis by the successive nucleation and glide of  $1/6 \langle 111 \rangle$  partial dislocations on adjacent  $\{112\}$  planes. Figure 8 shows the migration of initial twin boundary due to glide of  $1/6 \langle 111 \rangle$  partial dislocations, which leads to change in twin boundary spacing. Each nucleation, glide and annihilation of  $1/6 \langle 111 \rangle$  partial dislocation displaces the twin boundary by one layer. As a result of repeated nucleation and glide, the twin boundary migrates marginally along the nanopillar axis (Figure 6(d)). Although, the overall deformation is dominated by twinning mechanism (Figure 6(d)), minor activity of full dislocation slip is also observed in the neighbouring grain (Figure 6(c)). However, this full dislocation slip contributes negligibly to the overall strain. Similar to nanopillar having a single twin boundary, deformation by twinning occurs in nanopillars containing higher number of twin boundaries (Figure 9). However, few important differences were noticed in nanopillars containing two, three and five twin boundaries. It can be seen that in nanopillar containing two twin boundaries, the twinning occurs only in two grains and no activity of slip is observed in any grain (Figure 9(a)). Moreover, the operative twin systems in these two grains are symmetrical with respect to twin boundary. In contrast, in nanopillars containing three and five twin boundaries, considerable activity of full dislocations is also observed (Figure 9(b) and (c)). This full dislocation



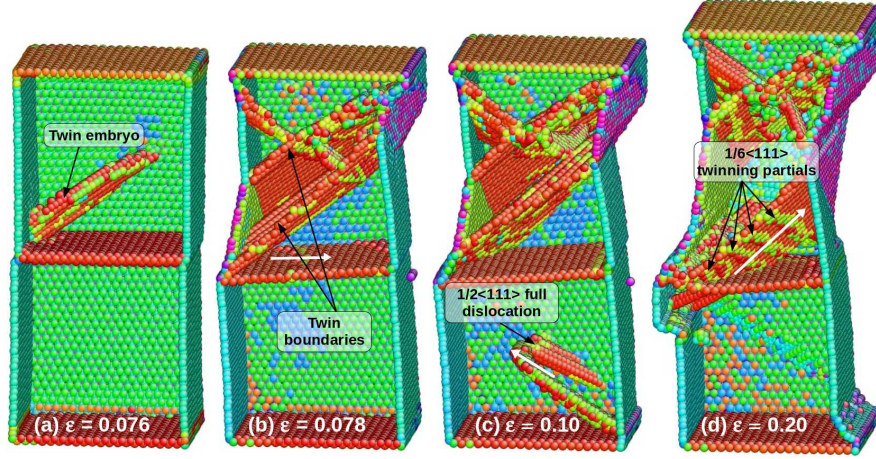


Figure 6: The deformation behaviour of BCC Fe nanopillar containing single twin boundary under tensile loading. The atoms are coloured according to the centro-symmetry parameter [27]. The perfect BCC atoms and the front surface are removed for clarity.

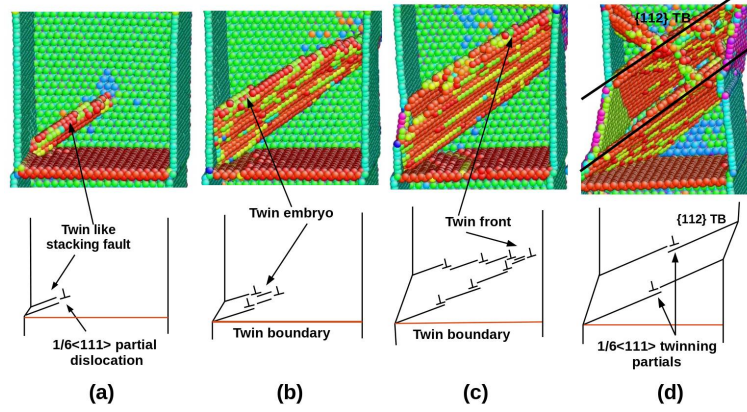


Figure 7: The detail process of twin embryo nucleation to twin boundary formation. The 2-D view of twin nucleation and growth is shown schematically in lower figures. The atoms are coloured according to the centro-symmetry parameter [27].

activity is aided by twin-twin interactions. Furthermore, the change in twin boundary spacing increases with increase in the number of twin boundaries. In addition, in nanopillars containing five twin boundaries, the twin boundary spacing has become uneven due to continuous glide of parallel twinning partials (Figure 9(c)). Upon increasing strain, the deformation is mainly concentrated at the twin boundaries in all the nanopillars, leading to the occurrence of necking close to one of the twin boundaries (Figure 9).

As the deformation under tensile loading of twinned nanopillars is dominated by twinning mechanism, it can offers an insights into twin-twin interactions. Figure 10 shows the twin-twin interactions under the tensile loading of twinned nanopillars observed in present study. Initially, the twin embryo consisting of many partial dislocations nucleates from the corner of the nanopillar and propagates towards the initial twin boundary (Figure 10(a)). The nucleated twin on  $[112]$  plane interacts with initial twin boundary on  $[\bar{1}\bar{1}\bar{2}]$  plane and produces  $\langle 012 \rangle$  twin-twin intersection (Figure 10(b)). In all the nanopillars undergoing twinning,  $\langle 012 \rangle$  type twin-twin intersections have been observed. Due to this twin-twin interaction, the formation of the twinning partials gliding along the twin boundary can be seen in Figure 10(b) and (c). The other possibility of twin-twin interactions arise from the pile-ups and combination of twinning partial dislocations (Figure 10(d)). During deformation, the



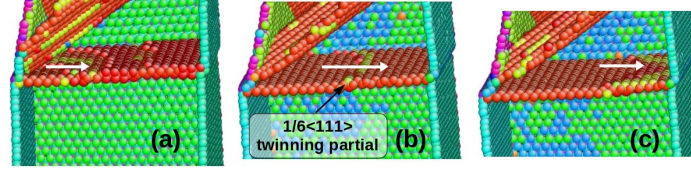


Figure 8: Typical glide of partial dislocations along the existing twin boundary. The continuous nucleation and glide of partial dislocations migrating the initial twin boundary is shown. The atoms are coloured according to the centro-symmetry parameter [27]. The perfect BCC atoms and the front surface are removed for clarity.

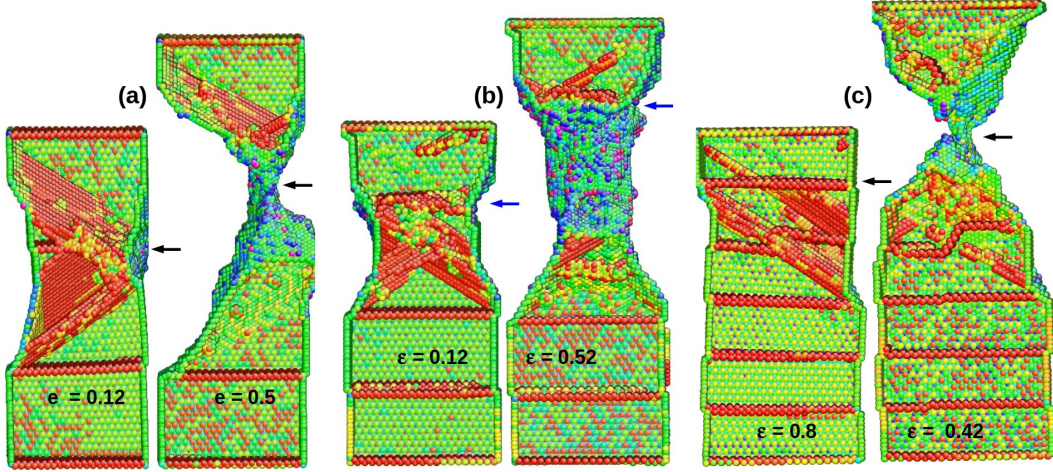


Figure 9: Deformation behaviour of BCC Fe nanopillars containing (a) two, (b) three and (c) five twin boundaries. The atoms are coloured according to the centro-symmetry parameter [27]. The perfect BCC atoms and the front surface are removed for clarity.

gliding twinning partials along the nucleated twin boundary pile-up against the initial twin boundary (Figure 10(d)). Following the pile-ups, three of twinning partials combine and form a full dislocation (Figure 10(e)). Upon increasing strain, the lattice near the twin-twin intersection is highly distorted (Figure 10(f)). The full dislocations thus nucleated, glide on the plane symmetrical with respect to the plane of nucleated deformation twin.

### 3.3 Deformation behaviour under compression

The deformation behaviour under the compressive loading of perfect and twinned BCC Fe nanopillars is dominated mainly by the slip of full dislocations. Figure 11 shows the deformation behaviour of perfect BCC Fe nanopillar oriented in  $\langle 112 \rangle$  axis under compressive loading. It can be seen that the yielding occurs by the nucleation of  $1/2\langle 111 \rangle$  full dislocations from the corner of the nanopillar (Figure 11(a)). Following yielding, the plastic deformation is entirely dominated by the slip of full dislocations. Due to glide of  $1/2\langle 111 \rangle$  screw dislocations, the straight and curved slip steps were observed on surface of the nanopillar (Figure 11(b)). Furthermore, the formation of large number of point defects can be seen in Figure 11(b). The non-conservative motion of dislocations leads to the creation of point defects such as vacancies and/or interstitials [32]. The typical atomic configurations representing plastic deformation under compressive loading of twinned nanopillars containing two twin boundaries are shown in Figure 12. The onset of yielding is characterised by the nucleation of dislocation loop originating from the corner of the nanopillar (Figure 12(a)). The DXA analysis [36] indicated that the dislo-

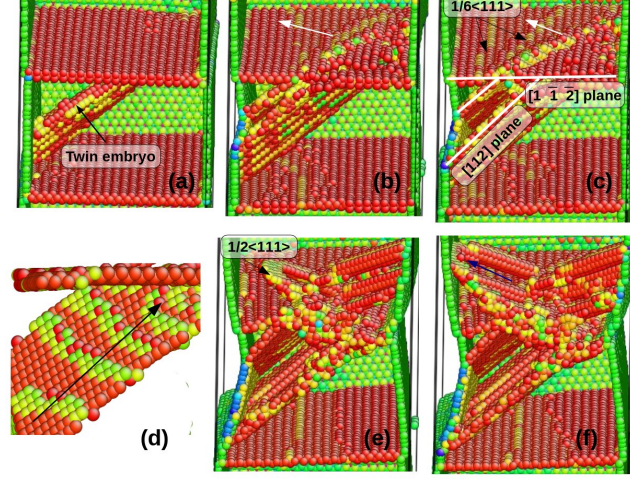


Figure 10: Twin-twin interaction under the tensile loading of twinned BCC Fe nanopillars. The nucleated twin on  $[11\bar{2}]$  plane interacts with the initial twin boundary on  $[\bar{1}\bar{1}2]$  plane and produces a  $\langle 012 \rangle$  type twin-twin intersection.  $\langle 012 \rangle$  twin-twin intersection is obtained as the cross product of  $(112)$  and  $(1\bar{1}\bar{2})$ . The full dislocation emission from the twin-twin interaction can be seen in (c) and (d). The atoms are coloured according to the centro-symmetry parameter [27]. The perfect BCC atoms and the front surface are removed for clarity.

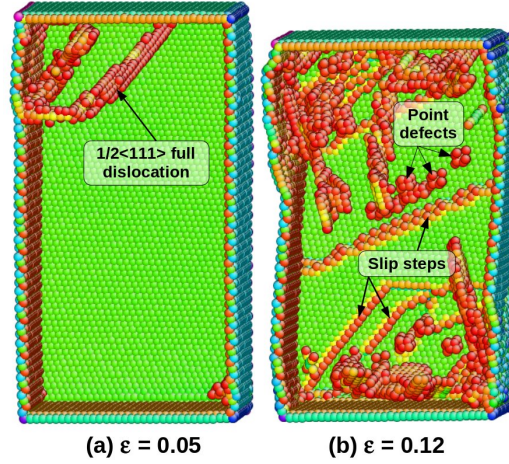


Figure 11: Deformation behaviour of perfect  $\langle 112 \rangle$  BCC Fe nanopillar under compressive loading. The atoms are coloured according to the centro-symmetry parameter [27]. The perfect BCC atoms and the front surface are removed for clarity.

cation loop has a Burgers vector  $1/2\langle 111 \rangle$  representing full dislocations in BCC system. Following nucleation, the dislocation loop expands in diameter and the part of the loop is annihilated at the free surface, while the remaining part is blocked at twin boundary (Figure 12(b)). This indicates that the twin boundaries in BCC Fe nanopillars are effective barriers for dislocation motion. With the increase in stress, the blocked dislocation penetrates the twin boundary and comes out as a loop in the next grain (Figure 12(c)). During this process of nucleation and propagation, the accumulation of large number of straight screw dislocations can be seen at higher strains in all the nanopillars (Figure 13(a)–(d)). The accumulation process of straight screw dislocations in BCC nanowires has also been demonstrated in our earlier investigation [32]. It has been observed that the dislocation loop initially nucleated from the corner consists of edge as well as screw components. In view of higher mobility of edge dislocations, the edge component of mixed dislocations easily escapes to the surface resulting in the accumulation of screw dislocations. In nanopillars containing one and two twin boundaries, accumulation



of long and straight screw dislocations has been observed (Figure 13(a) and (b)), while nanopillars having three and five twin boundaries, accrual of comparatively smaller screw dislocations have been noticed (Figure 13(c) and (d)). Furthermore, due to dislocation blockage by twin boundaries, the formation of hairpin-like dislocations has been observed during compressive deformation of twinned nanopillars with higher number of twin boundaries (Figure 13(d)). Generally, the dislocations that glide in hairpin-like configuration are known as hairpin dislocations and this kind of dislocations have also been observed in twinned FCC nanocrystalline materials [40].

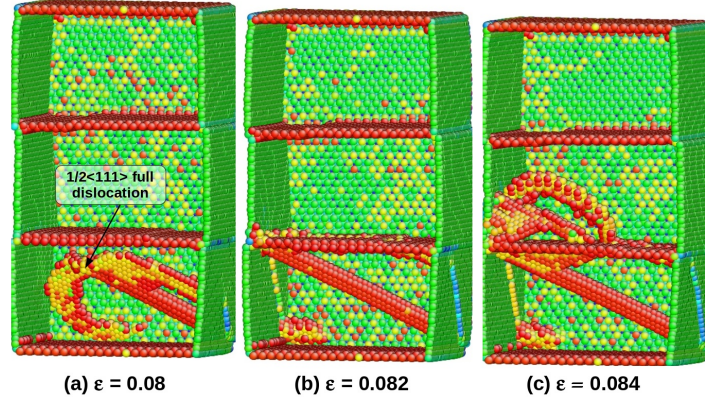


Figure 12: Deformation behaviour of BCC Fe nanopillar containing two twin boundaries under the compressive loading. The atoms are coloured according to the centro-symmetry parameter [27]. The perfect BCC atoms and the front surface are removed for clarity.

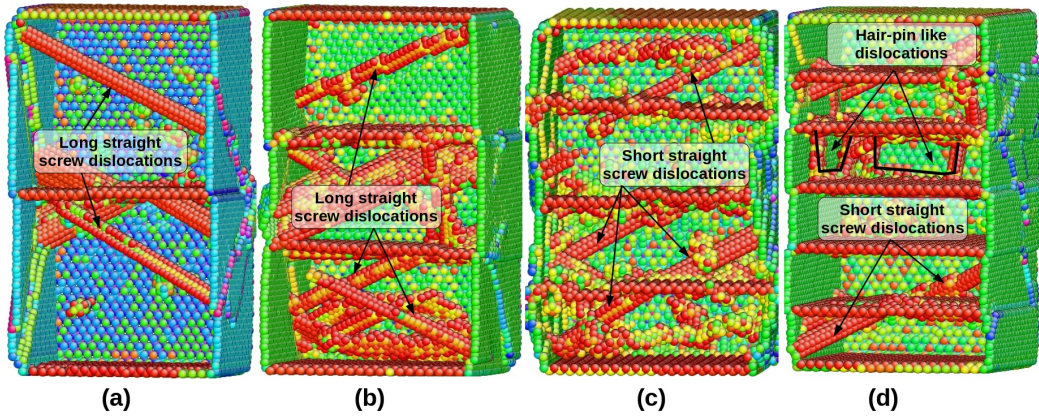


Figure 13: Accumulation of straight screw dislocations in the twinned BCC Fe nanopillars under the compressive loading. The atoms are coloured according to the centro-symmetry parameter [27]. The perfect BCC atoms and the front surface are removed for clarity.

Since the deformation of twinned nanopillars under the compressive loading is dominated by the full dislocations, it can offer an insight into dislocation-twin boundary interactions. In the present investigation, the dislocation-twin interactions have been observed for all the nanopillars under compressive loading. The direct transmission of  $1/2\langle 111 \rangle$  full dislocation across the twin boundary without any deviation in glide plane is shown in Figure 14. Initially,  $1/2\langle 111 \rangle$  full dislocation loop nucleates from the corner of nanopillar during yielding and grows with deformation (Figure 14(a)). Once the part of the dislocations reaches the twin boundary, the dislocation line becomes parallel to the intersection line of the glide plane and twin boundary (Figure 14(b)). With the increase in strain, this dislocation passes through the twin boundary and glides on the plane parallel to

the initial glide plane (Figure 14(c)). In addition to full dislocation directly transmitting through the twin boundary (Figure 14), another operating mechanism of dislocation transmission across the twin boundary is shown in Figure 15. In this case, the dislocation comes out of the twin boundary and glides on a plane symmetrical to the initial glide plane (Figure 15(a)–(c)).

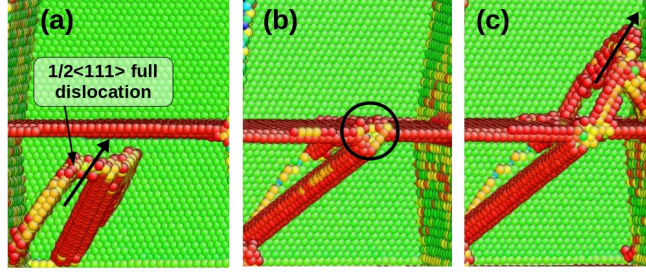


Figure 14: Dislocation-twin boundary interaction showing direct transmission of dislocation across the twin boundary. The viewing direction is  $\langle 111 \rangle$  and the atoms are coloured according to the centro-symmetry parameter [27]. The perfect BCC atoms and the front surface are removed for clarity.

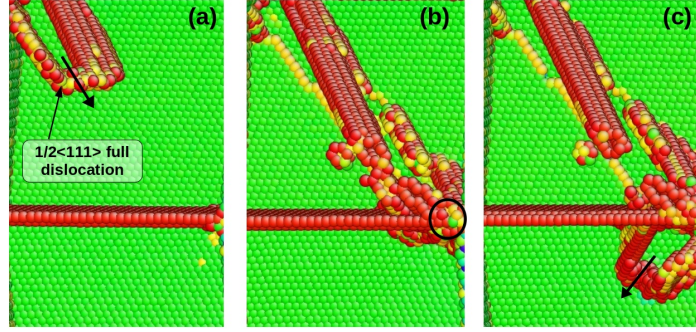


Figure 15: Dislocation-twin boundary interaction showing the symmetrical transmission of dislocation across the twin boundary. The viewing direction is  $\langle 111 \rangle$  and the atoms are coloured according to the centro-symmetry parameter [27]. The perfect BCC atoms and the front surface are removed for clarity.

### 3.4 Twin boundary as a dislocation source

Under the tensile deformation of twinned BCC Fe nanopillars, it has been observed that the nucleated twin boundary can often be of curved nature and edge of this curved twin boundary can acts as a source for nucleation of full dislocations. Figure 16 shows pictorial view of full dislocation emission from the curved twin boundary. Initially,  $1/6\langle 111 \rangle$  partial dislocation labelled as ‘1’ nucleates and glides along the curved twin boundary (Figure 16(a)). The motion of this partial dislocation is prevented at the edge of the twin boundary, and at the same time, another partial dislocation labelled as ‘2’ nucleates and approaches towards the edge of twin boundary (Figure 16(b)). These two partial dislocations combine and form a  $1/3\langle 111 \rangle$  partial dislocation labelled as ‘1 + 2’ in Figure 16(c). With a small increase in strain, one more  $1/6\langle 111 \rangle$  partial dislocation labelled as ‘3’ gets nucleated, and its subsequent glide and combination with the existing combined  $1/3\langle 111 \rangle$  partial dislocation leads to the formation of  $1/2\langle 111 \rangle$  full dislocation as shown in Figure 16(d). Thus, the nucleation of three successive partial dislocations and their pile up at the edge of the twin boundary leads to the formation of full dislocation. The  $1/2 \langle 111 \rangle$  full dislocation glide on  $\{110\}$  plane and moves away from the edge of the

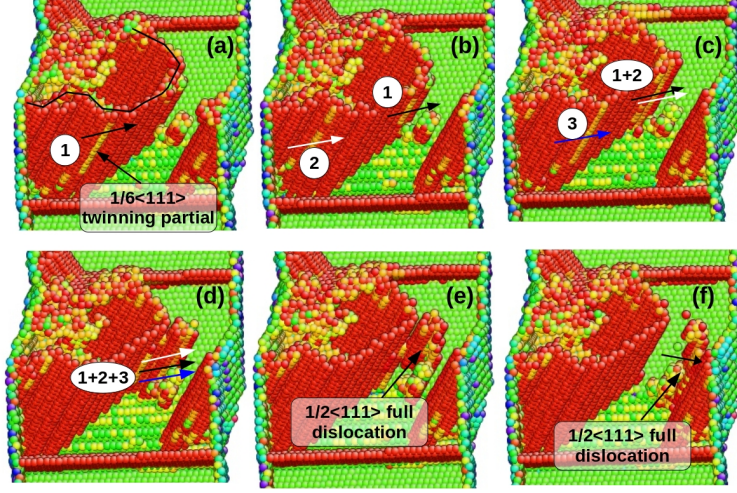


Figure 16: Process of full dislocation nucleation from the edge of curved twin boundary during tensile deformation of twinned BCC Fe nanopillar. The atoms are coloured according to the centro-symmetry parameter [27]. The perfect BCC atoms and the front surface are removed for clarity.

twin boundary. The nucleation of dislocation from the edge of the curved twin boundary is associated with the reduction in the thickness of twin (Fig. 16a-f).

## 4 Discussion

### 4.1 Non-linear elastic deformation

In tensile loading, all the nanopillars exhibited the non-linear elastic deformation at high elastic strains (Figure 2), while in compressive loading only twinned nanopillars displayed non-linear behaviour (Figure 4). The nanopillar without twin boundary under compressive loading showed perfectly linear elastic deformation (Figure 4). In the past, many atomistic simulations studies have shown that the elastic deformation of various FCC and BCC metallic nanowires is non-linear at high elastic strains under different loading conditions [33, 41]. The non-linear elastic deformation observed at high strains in the present investigation can be attributed to the nature of inter-atomic forces in BCC Fe nanowires [33]. At small atomic distances, the inter-atomic forces vary linearly with inter-atomic distance and this reflects in a linear elastic deformation at small strains. However, at higher atomic distances, the inter-atomic force varies non-linearly and this leads to the appearance of non-linear elastic deformation at high strains. Due to negligible defect density and high surface effects, the defect nucleation in the pristine nanowires requires high elastic strains compared to their bulk counterparts. As a result, the non-linear elastic deformation is observed mainly in materials at nanoscale. The observed non-linearity in elastic deformation results as a consequence of the ability of the nanowires to undergo large elastic deformation. In general, all the nanopillars under tensile and compressive loadings have shown large elastic strains except perfect nanopillar showing comparatively small elastic strain under compressive loading.



## 4.2 Effect of twin boundary spacing on yield stress

The yield stress as a function of twin boundary spacing exhibiting contrasting behaviour under tensile and compressive loadings has been observed in BCC Fe nanopillars. During tensile deformation, the yield stress displays negligible variation with respect to twin boundary spacing (Figures 2 and 3), while a significant decrease in yield strength with increasing twin boundary spacing has been observed under compressive loading (Figures 4 and 5). The observed variations in yield stress with respect to twin boundary spacing under tensile and compressive loadings are in agreement with those reported in twinned FCC nanopillars [12–15]. In twinned FCC nanopillars, the strengthening and negligible influence of twin boundary spacing was explained using the hard and soft modes of deformation [11, 42]. In BCC Fe nanopillars, this contrasting behaviour in the yield stress variations can arise mainly from the difference in yielding and subsequent plastic deformation mechanisms under tensile and compressive loadings. The observed deformation mechanisms are summarised schematically in Figure 17. Since the deformation under tensile loading is dominated by the twinning partial dislocations (Figures 6–9), the glide plane and the Burgers vector of this partials can either have an inclination or parallel with respect to twin boundary (Figure 17(a)). In case of an inclination, the repulsive force on the partial dislocations is smaller than that of full dislocations and as a result, the yield stress under tensile loading exhibits weaker dependence on twin boundary spacing. In other case, where the glide plane and the Burgers vector of partial dislocations are parallel to twin boundaries (Figure 17(a)), the twin boundary spacing has a insignificant role on yield stress due to negligible repulsive force [11, 42]. On the other hand, when the deformation is dominated by full dislocations under compressive loading (Figures 12 and 13), the slip plane and the Burgers vector of full dislocations have an inclination with respect to the twin boundary (Figure 17(b)). This mode of deformation is known as hard mode in FCC nanopillars [11]. In this mode, the twin boundaries exert strong repulsive force on full dislocations and also influence the resistance to dislocation slip. The repulsive force on the dislocations increases upon decreasing twin boundary spacing and as a result, the yield stress increases with the decrease in twin boundary spacing.

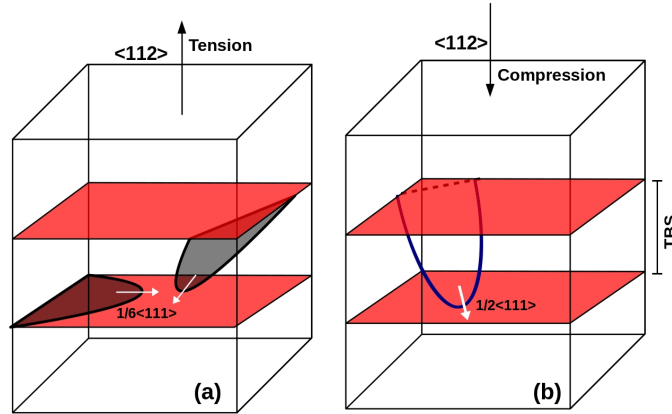


Figure 17: Schematic of the observed deformation mechanisms under (a) tensile and (b) compressive deformation of BCC Fe nanopillars.

The yield stress of twinned nanopillars under tensile loading is much lower than the yield stress of perfect nanopillar (Figure 3), while in compression the strength values are comparable for small spacing (i.e. nanopillars having three and five twin boundaries) and lower, for large spacing (Figure 5). This difference in yield stress



between perfect and twinned nanopillars arises mainly from the structure of twin boundary. With Mendelev EAM potential, the twin boundary in BCC Fe has a displaced or isosceles structure [31, 33, 34], where the upper grain is displaced with respect to the lower grain parallel to the boundary plane by the vector  $1/12\langle 111 \rangle$ . This extra step was observed experimentally in BCC Mo [43, 44], but not in BCC Fe. In BCC Fe, it has been reported that the twin boundary possesses a reflection structure [45, 46]. In twinned nanopillars, this extra step can act as a nucleation site for a twin embryo, while in perfect nanopillars, the twin embryo nucleates from the corner. Due to this extra step, the defect nucleation in the twinned nanopillars is easier than in perfect nanopillar. Under compressive loading, the observed low yield stress values for higher twin boundary spacing (i.e. nanopillars with one and two twin boundaries) can arise from the presence of such step. Further, the observed yield stress values for low twin boundary spacing (i.e. nanopillars with three and five twin boundaries) comparable to perfect nanopillar can be ascribed to the combined effects associated with repulsive force and step.

### 4.3 Flow stress and tension-compression asymmetry

Following yielding under tensile loading, the  $\langle 112 \rangle$  perfect nanopillar exhibits nearly constant low flow stress arising from the dominance of twin growth or twin boundary migration. It has been demonstrated that when the deformation is dominated by twinning mechanism in BCC Fe nanowires with  $\langle 100 \rangle$ ,  $\langle 112 \rangle$  and  $\langle 102 \rangle$  orientations, the twin growth/twin boundary migration remains a self-driven process and this results in nearly constant low flow stress [31, 33]. In general, deformation twinning spreads in the majority of gauge length in perfect nanopillars giving rise to large ductility. In twinned nanopillars, the gauge length portion participating during tensile deformation decreases with the increase in the number of twin boundaries or decrease in twin boundary spacing (Figures 6 and 9). As a result, the nanopillars containing one and two twin boundaries display gradual decrease in flow stress, well-defined necking and lower tensile ductility (Figures 2 and 9(a)). In case of nanopillars having three and five twin boundaries, more and more localised deformation leads to intense necking, rapid decrease in flow stress and further reduction in tensile ductility (Figures 2 and 9(b) and (c)). These results indicate that the presence of twin boundaries in BCC Fe nanopillars decreases the ductility compared to perfect nanopillars. In general, the twinned nanopillars exhibit flow stress fluctuations, which increases with increase in the number of twin boundaries particularly at low plastic strains (Figure 2). The observed flow stress fluctuations can be attributed to dislocation activity aided by twin-twin interactions occurring during plastic deformation (Figure 10(a)-(e)).

In contrast to tensile loading, the deformation is completely dominated by the slip of full dislocations and deformation spreads throughout the nanopillar gauge length under compressive loading. The twinning mechanism has not been observed during compressive deformation of perfect as well as twinned nanopillars. The continuous nucleation, glide and annihilation of full dislocations results in large flow stress fluctuations under compressive loading in the perfect nanopillar (Figure 4). In case of twinned nanopillars, in addition to continuous nucleation, glide and annihilation of full dislocations, dislocation-twin boundary interactions contribute to the observed flow stress fluctuations (Figures 4, 14 and 15). The observed tension-compression asymmetry in deformation mechanisms in terms of twinning under tensile loading and dislocation slip under the compressive loading is in agreement with those observed in  $\langle 100 \rangle$  BCC Fe nanowires [30, 33]. In BCC nanowires, tension-compression

asymmetry has been demonstrated for yield stress [33, 47] as well for the operating deformation mechanism [30, 33, 48]. It has been shown that the tension-compression asymmetry in deformation mechanisms in BCC Fe nanowires results as a consequence of twinning-antitwinning sense of  $1/6\langle 111 \rangle$  partial dislocations on  $\{112\}$  planes under the opposite loading conditions [30, 33, 47].

#### 4.4 Twin-twin and dislocation-twin interactions

The plastic deformation and the associated flow stress in polycrystalline materials are mainly controlled by the interaction between dislocations and grain boundaries. Here, we discuss the twin-twin and dislocation-twin interactions observed during deformation in the twinned nanopillars. In BCC metals, the twin-twin interactions have been classified based on their common line of intersection [39]. The observed  $\langle 021 \rangle$  type twin intersection is in agreement with the fact that in BCC metals, there are only five types of probable twin-twin intersections, namely  $\langle 011 \rangle$ ,  $\langle 012 \rangle$ ,  $\langle 113 \rangle$ ,  $\langle 111 \rangle$  and  $\langle 135 \rangle$  [39]. In  $\langle 021 \rangle$  type twin intersection, the  $1/2\langle 111 \rangle$  full dislocation may also originate in the neighbouring grain by the coalescence of  $1/6\langle 111 \rangle$  twinning partial dislocations (Figure 10(d)-(e)). Along with full dislocations, the nucleation of twinning partials gliding along the initial twin boundary leads to the twin boundary migration. In agreement with the present study, Ohja et al. [23] characterised  $\langle 110 \rangle$ ,  $\langle 113 \rangle$  and  $\langle 210 \rangle$  types twin-twin intersections in BCC Fe using experiments and molecular dynamics simulations.

The dislocation nucleation from the edge of curved twin boundary observed in the present investigation (Figure 16) is interesting, and this is in agreement with those obtained experimentally by Hull [49] in BCC Fe and Wang et al. [48] in BCC W using MD simulations. In BCC metals, the twin boundary or the twin-matrix interface can have different shapes such as lenticular, flame-like structure and complicated fine structure of serrations [50]. The edges or the serrations can act as a stress concentration site. In order to relieve this localised stress, full dislocation nucleates from the edges of the curved twin boundary and glide on  $\{110\}$  plane [49].

The dislocation-twin boundary interactions during deformation under compressive loading reveal that the dislocation can either directly transmit through the twin boundary without any deviation in the glide plane (Figure 14) or it can transmit to symmetrical plane in the neighbouring grain (Figure 15). Mrovec et al. [22] examined the dislocation-twin boundary interactions in BCC tungsten using Finnis-Sinclair and bond order potential. Depending on inter-atomic potential, dislocation character and its glide plane, various reactions such as dislocation splitting into three twinning partials along the twin boundary, twin boundary destruction and disintegration close to absorption site, the dislocation embedding in the twin boundary, and the direct transmission of the dislocations have been observed [22]. In BCC metals, three  $\{112\}$  and three  $\{110\}$  planes have the same  $\langle 111 \rangle$  zone axis (Figure 18(a)). Interestingly, this arrangement of glide planes remains the same across the twin boundary (Figure 18(b)). In view of this similarity in the slip planes, dislocation once passes through the twin boundary can either glide on symmetrical plane or can directly come out in the neighbouring grain without any deviation in the glide plane. The inserted atomic snapshots in Figure 18(b) show that the observed slip lines in Figures 14 and 15 are parallel to  $\{112\}$  planes. The geometrical arrangement of glide plane (Figure 18(b)) indicates that the observed dislocation-twin boundary interactions in the present study are on expected lines in BCC metals.

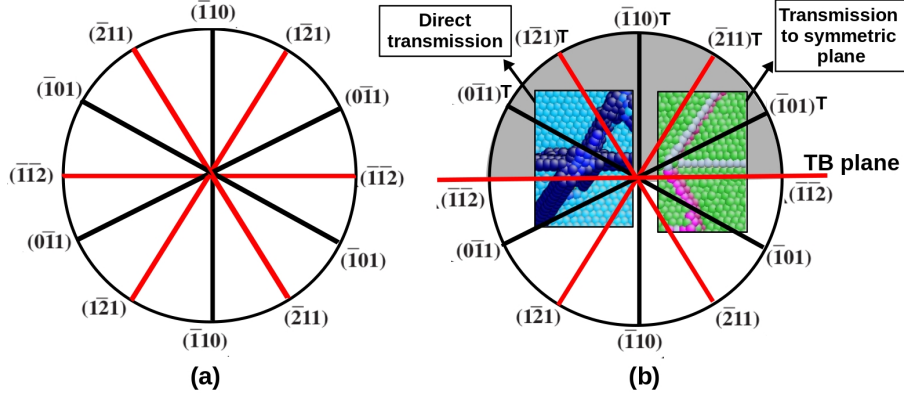


Figure 18: The arrangement of three  $\{110\}$  and three  $\{112\}$  planes having the same  $\langle 111 \rangle$  zone axis in BCC metal in (a) perfect and (b) across the twin boundary in twinned crystals.

#### 4.5 Comparison with experimental data and effect of inter-atomic potential

The most important aspect of atomistic simulations is the reliability of inter-atomic potential. Generally, the EAM potentials are more reliable for many FCC systems, while for BCC systems they are comparatively less accurate in reproducing the defect structures, slip systems, twinning behaviour and phase transition. This is mainly because the non-planar core of screw dislocations in BCC systems makes the slip more complex compared to FCC systems. Furthermore, the atomistic simulations on various BCC systems have suggested that the activated slip systems and the deformation mechanisms depends sensitively on inter-atomic potential employed in simulations [51–53]. For example in BCC Fe, Mendelev EAM potential employed in the present investigation shows non-degenerate core for screw dislocations and predicts  $\{112\}$  and  $\{110\}$  as glide planes [53]. Contrary to this, Simmonelli potential [52] shows degenerate core for screw dislocations and predicts only  $\{112\}$  glide plane [53]. However, recent experimental results have shown that the glide is observed on  $\{110\}$  planes in BCC Fe [54]. In this context, it is more important to understand that up to what degree the predictions made in the present investigation differ with potential. Cao [55] in his study on shape memory and pseudo-elasticity of  $\langle 100 \rangle$  BCC Fe nanowires has shown that under tensile deformation, the qualitative stress-strain behaviour and deformation by twinning doesn't vary significantly with Mendelev [28] and Chamati [56] potentials. However, these two potentials predict different values of yield stress [55]. On similar lines, the quantitative values of yield stress predicted in the present investigation may vary with inter-atomic potential, but the qualitative aspects may not change significantly although it needs further investigations.

In the present study, we have chosen Mendelev EAM potential mainly because several predictions made with this potential are in good agreement with either experimental observations or density functional theory calculations. The first and foremost is the Mendelev EAM potential predicting a non-degenerate core structure for screw dislocations spreading symmetrically on three  $\{110\}$  planes of  $\langle 111 \rangle$  zone [53]. This is in agreement with density functional theory calculations [57]. All other potentials including Chamati [56] and Simonelli [52] potentials for BCC Fe predicts a degenerate core structure spreading asymmetrically on three  $\{110\}$  planes [53]. Similarly, the predictions made in the present investigation on deformation twinning and dislocation slip in BCC Fe nanopillars are quite close to the experimental observations in BCC W nanopillars [48]. Using in situ transmission electron microscopy in BCC W nanopillars, Wang et al. [48] predicted deformation twinning

for  $\langle 100 \rangle$ -tension,  $\langle 110 \rangle$  and  $\langle 111 \rangle$ -compression, while dislocation slip is observed for  $\langle 112 \rangle$ -tension and compression. In agreement with this experimental study, the Mendelev EAM potential predicts deformation twinning for  $\langle 100 \rangle$ -tension and  $\langle 110 \rangle$ -compression and dislocation slip for  $\langle 112 \rangle$ -compression in BCC Fe nanowires/nanopillars [33]. However, it predicts twinning for  $\langle 112 \rangle$ -tension [33], which is in contrast with the experimental observations [48]. Similarly, the mechanism of twin nucleation and growth, and twin boundary as a source of full dislocation nucleation observed in the present investigation using Mendelev EAM potential are in agreement with those observed experimentally [48, 49]. Further, in agreement with experimental results, the MD simulation results using Mendelev EAM potential also described the various twin-twin interactions and twin migration stress in BCC Fe [23].

## 5 Conclusions

Molecular dynamics simulations performed on twinned BCC Fe nanopillars indicated that the twin boundaries have a contrasting role under tensile and compressive loadings. Under tensile loading, the yield stress has been almost independent of twin boundary spacing, while under compressive loading, the yield stress showed strong dependence on twin boundary spacing. This contrasting behaviour in yield stress has been explained by repulsive force offered by the twin boundaries. Under tensile loading, deformation is dominated by the twin growth/twin boundary migration, where the initial twin boundary offers negligible repulsive force on the nucleation of twinning partials. Due to this, yield stress varies marginally as a function of twin boundary spacing. In addition to twinning, minor activity of full dislocations and twin-twin interactions of  $\langle 021 \rangle$  type have been observed during tensile deformation. It has been found that the edge of the curved twin boundary can act as a source for the emission of full dislocations. It has been observed that the deformation under compressive loading is dominated by the slip of full dislocations, where the twin boundaries offer a strong repulsive force for the nucleation of full dislocations. This leads to the observed strong dependence of yield stress on twin boundary spacing. The dislocation-twin boundary interactions obtained under the compressive deformation of twinned nanopillars revealed that the dislocation can either directly transmit without any deviation in slip plane or it can transmit on symmetrical slip plane in the neighbouring grain.

## References

- [1] L. Lu, X. Chen, X. Huang, and K. Lu, Revealing the maximum strength in nanotwinned copper, *Science* 323 (2009) 607-610.
- [2] X. Li, Y. Wei, L. Lu, L. Lu, and H. Gao, Dislocation nucleation governed softening and maximum strength in nano-twinned metals, *Nature* 464 (2010) 877-880.
- [3] J. Wang, F. Sansoz, J. Huang, Y. Liu, S. Sun, Z. Zhang, and S.X. Mao, Near-ideal theoretical strength in gold nanowires containing angstrom scale twins, *Nat. Commun.* 4 (2013) 1742.
- [4] E.W. Qin, L. Lu, N.R. Tao, and K. Lu, Enhanced fracture toughness of bulk nanocrystalline Cu with embedded nanoscale twins, *Scr. Mater.* 60 (2009) 539-542.

- [5] A. Singh, L. Tang, M. Dao, L. Lu, and S. Suresh, Fracture toughness and fatigue crack growth characteristics of nanotwinned copper, *Acta Mater.* 59 (2011) 2437-2446.
- [6] L. Liu, J. Wang, S.K. Gong, and S.X. Mao, Atomistic observation of a crack tip approaching coherent twin boundaries, *Sci. Rep.* 4 (2014) 4397.
- [7] C. Deng and F. Sansoz, Effects of twin and surface facet on strain-rate sensitivity of gold nanowires at different temperatures, *Phys. Rev. B* 81 (2010) 155430.
- [8] O. Anderoglu, A. Misra, H. Wang, and X. Zhang, Thermal stability of sputtered Cu films with nanoscale growth twins, *J. Appl. Phys.* 103 (2008) 094322.
- [9] J. Wang, N. Li, and A. Misra, Structure and stability of  $\Sigma 3$  grain boundaries in face centered cubic metals, *Philos. Mag.* 93 (2012) 315-327.
- [10] L. Lu, Y. Shen, X. Chen, L. Qian, and K. Lu, Ultrahigh strength and high electrical conductivity in copper, *Science* 304 (2004) 422-426.
- [11] T. Zhu and H. Gao, Plastic deformation mechanism in nanotwinned metals: An insight from molecular dynamics and mechanistic modeling, *Scr. Mater.* 66 (2012) 843-848.
- [12] A.J. Cao, Y.G. Wei, and S.X. Mao, Deformation mechanisms of face-centered-cubic metal nanowires with twin boundaries, *Appl. Phys. Lett.* 90 (2007) 151909.
- [13] Y. Zhang and H. Huang, Do twin boundaries always strengthen metal nanowires?, *Nanoscale Res. Lett.* 4 (2009) 34-38.
- [14] F. Hammami and Y. Kulkarni, Size effects in twinned nanopillars, *J. Appl. Phys.* 116 (2014) 033512.
- [15] Y. Wei, Anisotropic size effect in strength in coherent nanowires with tilted twins, *Phys. Rev. B* 84 (2011) 014107.
- [16] G. Sainath and B.K. Choudhary, Molecular dynamics simulation of twin boundary effect on deformation of Cu nanopillars, *Phys. Lett. A* 379 (2015) 1902-1905.
- [17] J.P. Hirth, J. Lothe, *Theory of Dislocations*, McGraw-Hill, New York, 1968.
- [18] Y. Shibuta, S. Takamoto, and T. Suzuki, A molecular dynamics study of the energy and structure of the symmetric tilt boundary of iron, *ISIJ Inter.* 48 (2008) 1582-1591.
- [19] M. Yamaguchi and V. Vitek, Twin boundaries and incoherent steps on twin boundaries in body centered-cubic metals, *Philos. Mag.* 34 (1976) 1-11.
- [20] T. Ezaz, M.D. Sangid, and H. Sehitoglu, Energy barriers associated with slip-twin interactions, *Philos. Mag.* 91 (2011) 1464-1488.
- [21] Y.T. Zhu, X.L. Wu, X.Z. Liao, J. Narayan, L.J. Kecskes, and S.N. Mathaudhu, Dislocation-twin interactions in nanocrystalline fcc metals, *Acta Mater.* 59 (2011) 812-821.
- [22] M. Mrovec, C. Elsasser, and P. Gumbsch, Interactions between lattice dislocations and twin boundaries in tungsten: A comparative atomistic simulation study, *Philos. Mag.* 89 (2009) 3179-3194.
- [23] A. Ojha, H. Sehitoglu, L. Patriarca, and H.J. Maier, Twin migration in Fe-based bcc crystals: Theory and experiments, *Philos. Mag.* 94 (2014) 1816-1840.

- [24] L. Wang, F. Zhao, F.P. Zhao, Y. Cai, Q. An, and S.N. Luo, Grain boundary orientation effects on deformation of Ta bicrystal nanopillars under high strain-rate compression, *J. Appl. Phys.* 115 (2014) 053528.
- [25] S. Plimpton, Fast parallel algorithms for short-range molecular dynamics, *J. Comp. Phys.* 117 (1995) 1-19.
- [26] J. Li, Atom eye: An efficient atomistic configuration viewer, *Modell. Simul. Mater. Sci. Eng.* 11 (2003) 173.
- [27] C.L. Kelchner, S.J. Plimpton, and J.C. Hamilton, Dislocation nucleation and defect structure during surface indentation, *Phys. Rev. B* 58 (1998) 11085-11088.
- [28] M.I. Mendelev, S. Han, D.J. Srolovitz, G.J. Ackland, D.Y. Sun, and M. Asta, Development of new interatomic potentials appropriate for crystalline and liquid iron, *Phil. Mag.* 83 (2003) 3977-94.
- [29] S. Kotrechko and A. Ovsjannikov, Temperature dependence of the yield stress of metallic nanosized crystals, *Philos. Mag.* 89 (2009) 3049-3058.
- [30] C.J. Healy and G.J. Ackland, Molecular dynamics simulations of compression-tension asymmetry in plasticity of Fe nanopillars, *Acta Mater.* 70 (2014) 105-112.
- [31] G. Sainath, B.K. Choudhary, and T. Jayakumar, Molecular dynamics simulation studies on the size dependent tensile deformation and fracture behaviour of body centred cubic iron nanowires, *Comp. Mater. Sci.* 104 (2015) 76-83.
- [32] G. Sainath and B.K. Choudhary, Molecular dynamics simulations on size dependent tensile deformation behaviour of [110] oriented body centred cubic iron nanowires, *Mater. Sci. Eng. A* 640 (2015) 98-105.
- [33] G. Sainath and B.K. Choudhary, Orientation dependent deformation behaviour of BCC iron nanowires, *Comp. Mater. Sci.* 111 (2016) 406-415.
- [34] Z. Shi and C.V. Singh, Competing twinning mechanisms in body-centered cubic metallic nanowires, *Scr. Mater.* 113 (2016) 214-217.
- [35] J.A. Zimmerman, E.B. Webb, J.J. Hoyt, R.E. Jones, P.A. Klein, and D.J. Bammann, Calculation of stress in atomistic simulation, *Modell. Simul. Mater. Sci. Eng.* 12 (2003) S319-S332.
- [36] A. Stukowski and K. Albe, Dislocation detection algorithm for atomistic simulations, *Modell. Simul. Mater. Sci. Eng.* 18 (2010) 025016.
- [37] A. Stukowski, Visualization and analysis of atomistic simulation data with OVITO-the Open Visualization Tool, *Modell. Simul. Mater. Sci. Eng.* 18 (2009) 015012.
- [38] H.W. Paxton, Experimental verification of the twin system in alpha-iron, *Acta Metall.* 1 (1953) 141-143.
- [39] S. Mahajan, Accommodation at deformation twins in bcc crystals, *Metall. Trans. A* 12 (1981) 379-386.
- [40] Y. Zhu, Z. Li, M. Huang, and Y. Liu, Strengthening mechanisms of the nanolayered polycrystalline metallic multilayers assisted by twins, *Int. J. Plast.* 72 (2015) 168-184.
- [41] I. Salehinia and D. Bahr, Crystal orientation effect on dislocation nucleation and multiplication in FCC single crystal under uniaxial loading, *Int. J. Plast.* 52 (2014) 133-146.
- [42] Z. You, X. Li, L. Gui, Q. Lu, T. Zhu, H. Gao, and L. Lu, Plastic anisotropy and associated deformation mechanisms in nanotwinned metals, *Acta Mater.* 61 (2013) 217-227.



- [43] S. Tsurekawa, T. Tanaka, and H. Yoshinaga, Grain boundary structure, energy and strength in molybdenum, *Mater. Sci. Eng. A* 176 (1994) 341-348.
- [44] T. Vystavel, J.M. Penisson, and A. Gemperle, High-resolution and conventional electron microscopy study of a  $\Sigma = 3, [101]\{121\}$  twin grain boundary in molybdenum, *Philos. Mag. A* 81 (2001) 417-429.
- [45] K. Marukawa, A study of the atomic structure of twin boundaries in body-centred cubic crystals by electron microscopy, *Philos. Mag.* 36 (1977) 1375-1383.
- [46] C.T. Forwood and L.M. Clarebrough, Rigid body displacements at a faceted  $\Sigma 3$  boundary in  $\alpha$ -iron, *Phys. Status Solidi A* 105 (1988) 365-375.
- [47] J.Y. Kim, D. Jang, and J.R. Greer, Crystallographic orientation and size dependence of tension-compression asymmetry in molybdenum nanopillars, *Int. J. Plast.* 28 (2012) 46-52.
- [48] J. Wang, Z. Zeng, C.R. Weinberger, Z. Zhang, T. Zhu, and S.X. Mao, In situ atomic-scale observation of twinning-dominated deformation in nanoscale body-centred cubic tungsten, *Nat. Mater.* 14 (2015) 594-600.
- [49] D. Hull, The initiation of slip at the tip of a deformation twin in  $\alpha$ -iron, *Acta Metall.* 9 (1961) 909-911.
- [50] C. N. Reid, A review of mechanical twinning in body centred cubic metals and its relation to brittle fracture, *J. Less Common Metals* 9 (1965) 105-122.
- [51] L.M. Hale, J.A. Zimmerman, and C.R. Weinberger, Simulations of bcc tantalum screw dislocations: Why classical inter-atomic potentials predict  $\{112\}$  slip, *Comput. Mater. Sci.* 90 (2014) 106-115.
- [52] G. Simonelli, R. Pasianot, and E. Savino, Embedded-atom-method interatomic potentials for bcc-iron, *Mater. Res. Soc. Symp. Proc.* 291 (1993) 567-572.
- [53] J. Chaussidon, M. Fivel, and D. Rodney, The glide of screw dislocations in bcc Fe: Atomistic static and dynamic simulations, *Acta Mater.* 54 (2006) 3407-3416.
- [54] D. Caillard, Kinetics of dislocations in pure Fe. Part I. In situ straining experiments at room temperature, *Acta Mater.* 58 (2010) 3493-3503.
- [55] A. Cao, Shape memory effects and pseudoelasticity in bcc metallic nanowires, *J. Appl. Phys.* 108 (2010) 113531.
- [56] H. Chamati, N.I. Papanicolaou, Y. Mishin, and D.A. Papaconstantopoulos, Embedded-atom potential for Fe and its application to self-diffusion on Fe(100), *Surf. Sci.* 600 (2006) 1793-1803.
- [57] S.L. Frederiksen and K.W. Jacobsen, Density functional theory studies of screw dislocation core structures in bcc metals, *Philos. Mag.* 83 (2003) 365-375.